A New Photometric Redshift Method for Galaxies with 0.01 < z < 0.03

Jackson Steele

A senior thesis submitted to the faculty of
Brigham Young University
in partial fulfillment of the requirements for the degree of

Bachelor of Science

Michael D. Joner and J Ward Moody, Advisors

Department of Physics and Astronomy

Brigham Young University

April 2021

ABSTRACT

A New Photometric Redshift Method for Galaxies with $0.01 < z < 0.03$

Jackson Steele
Department of Physics and Astronomy, BYU
Bachelor of Science

We typically measure the redshift for distant galaxies using spectroscopy. Although spectroscopy is highly accurate, it requires the use of large telescopes (the time on which is limited). Photometric redshift, another technique, is highly imprecise but can be done on much smaller telescopes. We have created a new method to measure redshift photometrically that is an order of magnitude more precise than other photometric redshift techniques. To do this, we use three specialized narrow-band filters: two filters with variable (linear) transmission that are sloped oppositely (called 'ramp' filters), and a third 21nm FWHM filter to measure the continuum. These isolate the Hα emission-line for galaxies with $0.01 < z < 0.03$. Because the transmission is variable in our ramp filters, the brightness of Hα in each filter is a function of the redshift. We have tested this method observationally with 16 Seyfert galaxies and computationally with 197 emission-line galaxies. We are able to predict the redshift with a standard error of 572 km s^{-1}. This error decreases for galaxies with stronger Hα emission, and we find that the error drops to 252 km s^{-1} if the Hα equivalent width is over 40Å.

Keywords: photometric redshift, SDSS, distance measurements

ACKNOWLEDGMENTS

I would like to acknowledge the help and support of my advisors, Dr. Moody and Dr. Joner. They provided the guidance that made this research possible. I would also like to acknowledge all of the students who worked on this project before me and paved the way for my research. In addition, I would like to thank the Brigham Young University Department of Physics and Astronomy for funding this research.

I would also be remiss not to thank my wonderful wife Rochelle, whom I met and married during the course of this research and who has been my constant support. I am also grateful to my parents for raising me and to my firstborn child who has graciously decided to be born after the completion of this thesis.

Funding for the SDSS and SDSS-II has been provided by the Alfred P. Sloan Foundation, the Participating Institutions, the National Science Foundation, the U.S. Department of Energy, the National Aeronautics and Space Administration, the Japanese Monbukagakusho, the Max Planck Society, and the Higher Education Funding Council for England. The SDSS Web Site is http://www.sdss.org/.

The SDSS is managed by the Astrophysical Research Consortium for the Participating Institutions. The Participating Institutions are the American Museum of Natural History, Astrophysical Institute Potsdam, University of Basel, University of Cambridge, Case Western Reserve University, University of Chicago, Drexel University, Fermilab, the Institute for Advanced Study, the Japan Participation Group, Johns Hopkins University, the Joint Institute for Nuclear Astrophysics, the Kavli Institute for Particle Astrophysics and Cosmology, the Korean Scientist Group, the Chinese Academy of Sciences (LAMOST), Los Alamos National Laboratory, the Max-Planck-Institute for Astronomy (MPIA), the Max-Planck-Institute for Astrophysics (MPA), New Mexico State University, Ohio State University, University of Pittsburgh, University of Portsmouth, Princeton University, the United States Naval Observatory, and the University of Washington.

Contents

List of Figures

Chapter 1

Introduction

Extragalactic astronomy relies on accurate distance measurements to map out the Universe and determine likely formation theories. However, it is incredibly difficult and time-consuming to obtain these distance measurements. We have developed a more accessible and precise method to measure distance using a set of photometric filters with sloped transmission values. Computational simulations indicate that this technique works with a standard deviation of 572 km s^{-1}. Our precision improves with increasing equivalent width of the Hα line ($\lambda = 656.3$ nm).

1.1 Motivation

Throughout the many sub-disciplines of astronomy, distance is a crucial measurement that is frequently difficult to ascertain. Although there are methods used to find distances to each astronomical object, they are typically not interchangeable. For example, we can find distances to stars by using their motion throughout the year relative to more distant background stars. This method is called parallax, and it is incredibly useful for nearby stars. However, galaxies are at distances so great that their motion (compared to background galaxies) is negligible, rendering the parallax method essentially useless for these objects. Even the methods used to measure distance to nearby galaxies do not work for more distant galaxies and vice versa.

Those of us that study galaxies outside our own want to know these distances for several reasons. One major reason is to understand the nature of dark matter and the formation of the Universe. Using galactic distances, we create maps that outline how the Universe is structured. We find that galaxies formed in groups, creating large clusters with thin filaments connecting these clusters, surrounding massive voids that appear completely empty. However, our best theories about the nature of dark matter predict the presence of dwarf galaxies in the centers of these voids. So far, no dwarf galaxy has ever been discovered that resided within a void. As we shall soon see, the main distance measurement techniques are not well-suited to finding these dim galaxies. In response, we are developing our own method that is designed to work well for these dwarf galaxies.

1.2 Measuring Redshift

A term that I will use synonymously with distance is 'redshift'. This term comes from the apparent reddening that happens to light as it travels through space. As the Universe expands, the light passing through it is stretched as well, giving it a longer (redder) wavelength. This reddening is a function of distance, which means that we can find the distance to a galaxy given how red the light is. This should not be confused with the extinction and reddening of light passing through the interstellar medium, where short wavelength light is absorbed and scattered easier than the longer wavelengths. The equation to measure this redshift (or z), is as follows:

$$z = \frac{\lambda_{obs} - \lambda_{emitted}}{\lambda_{emitted}} \tag{1.1}$$

In this equation, λ_{obs} is the observed (redshifted) wavelength, whereas $\lambda_{emitted}$ is the original wavelength of the light when it was emitted from the source. Sometimes, this unitless number z is replaced instead with cz, or the redshift z multiplied by the speed of light c. This results in units of km s^{-1}. Because of this conversion, extragalactic distances are expressed interchangeably in terms of either redshift or velocity.

1.2.1 Spectroscopy

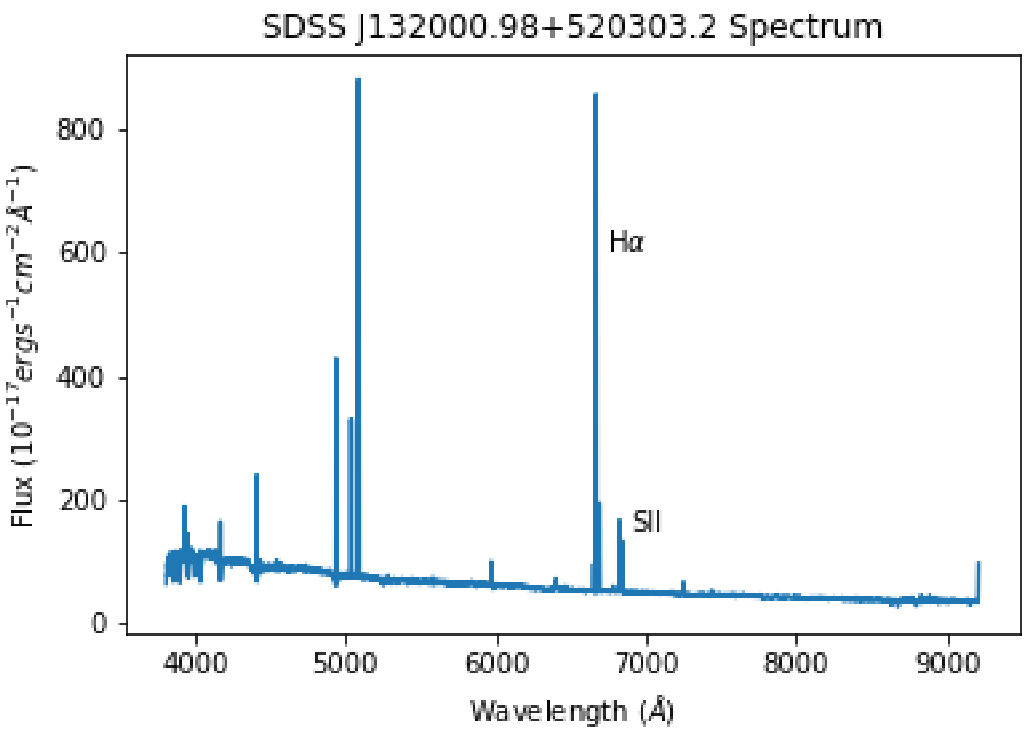

Figure 1.1 This is a sample spectrum of a typical emission-line galaxy (SDSS J123000.98+520303.2), using data obtained from the Sloan Digital Sky Survey (SDSS) DR7 (Abazajian et al. 2009). Two prominent emission lines are labeled: the Hα line that we looked for in our ramp filters, as well as the [SII] line that increased our errors for high-redshift galaxies.

By passing light through a prism or grating, we can measure the relative flux of the light as a function of wavelength. This process is called spectroscopy. When we take the light from a galaxy, for example, and pass it through a prism, we see certain identifiable spectral features (as in Fig. 1.1). These correspond to atoms (e.g., hydrogen or oxygen) which are found in the galaxy observed. By heating up these atoms in a laboratory and measuring the emitted light, we find the original wavelength of light when it was emitted from the galaxy. By comparing this to the wavelength we measured using Eq. 1.1, we can find the distance.

Spectroscopy is accurate, but it takes large amounts of light to be able to split it into component wavelengths. Gathering enough light requires using large telescopes (of which there are few and on which time is limited), and works better for bright objects (unlike distant dwarf galaxies). Additionally, spectroscopy is usually performed on one object at a time, and is not ideal for survey work.

1.2.2 Photometry

Photometry consists of taking images of objects through a telescope using specialized filters, then comparing these images to each other to gain insights. These filters transmit light at specific wavelengths while blocking all the light in other regions of the spectrum. Photometric measures of redshift rely on correlations between the brightness through certain filters to the redshift.

This is preferable over spectroscopy because it uses much smaller (and more readily available) telescopes, as well as working for multiple objects at once. However, these methods tend to have higher levels of error than spectroscopy.

The first photometric redshift method was developed by Baum (1962), which has since led to many other methods, including color-color diagrams (Koo (1985), Pello et al. (1996), Bolzonella et al. (2000)), linear regression (Connolly et al. 1995), template fitting (Loh & Spillar 1986), prediction trees (Carrasco Kind & Brunner 2013), and neural networks (Collister & Lahav 2004). In addition to these methods, we note that Beck et al. (2016) used an empirical template method alongside SDSS data. Unfortunately, their standard of error (6150 km s^{-1}) was similar in size to the voids we are working with, making their method unusable for void research.

In order to marry the benefits of spectroscopy and photometry, our team has designed a set of narrow-band filters (called 'ramp' filters) with variable transmission values that focus on the Hα

emission line in galaxies with $0.01 < z < 0.03$ (Lesser et al. 2019). Because we are only trying to measure the distance to these galaxies (and do not need to see all of their spectral features), isolating this emission line allows us to conduct a photometric analog to spectroscopy, identifying the observed wavelength of this Hα line. By doing this, we have improved the precision by an order of magnitude (standard deviation of 572 km s^{-1}), which makes it possible to conduct a survey of dwarf galaxy redshift to find any dwarf galaxies that might reside in the void.

1.2.3 Other Galactic Distance Measurements

Depending on the galaxy being observed, there are several other possible methods used to find the redshift. Each of these methods relies on comparisons between the absolute magnitude (or the brightness of the galaxy from a standard distance) and the apparent magnitude (or the brightness of the galaxy that we observe from Earth). These are related by the inverse-square law, which states that the apparent brightness is proportional to the absolute brightness divided by the distance squared.

All Type Ia supernovae (the explosion of a white dwarf star once it accretes enough mass to restart nuclear fusion) have approximately the same absolute magnitude at maximum light. Because of this, whenever a Type Ia supernova is observed in a distant galaxy, the absolute magnitude is immediately known. The apparent magnitude is measured with a telescope, and a comparison of the two using the inverse-square law provides the distance.

Another method is to use the Period-Luminosity relationship of Cepheid variable stars, which relates the period of a Cepheid to its absolute magnitude (Leavitt 1908). Again, after measuring the period and the apparent magnitude, a comparison of the apparent magnitude of a Cepheid in a distant galaxy with its known absolute magnitude will determine the distance.

For spiral galaxies, we can also use the Tully-Fisher Relation, which relates the width of emission lines with the total luminosity of a galaxy (Tully et al. 1975). If the total luminosity is known, then this can be compared to the apparent magnitude to get a distance measurement.

These methods are highly useful and have been used to calibrate the relationship between redshift and distance. However, because of the nature of the dwarf galaxies we hope to study, it is not practical to use these methods.

Chapter 2

Methods

To measure redshift photometrically for galaxies with $0.01 < z < 0.03$, we decided to focus on the Hα emission line. We made this decision because the Hα line is a common, prominent spectral feature among galaxies. We created a set of three narrow-band photometric filters, for which the brightness in two of them is a function of the Hα line's wavelength. The ratio of these two filters correlates with redshift, meaning we can use these filters to accurately measure distance.

2.1 Filter Setup

We used three specialized photometric filters in our design. Two of these filters cover the same wavelength range (655-685 nm) but their transmission levels are sloped oppositely. The first is called the "blue-sloping" or "BS" filter. This would ideally have 100% transmission at 655 nm and decrease linearly down to 0% transmission at 685 nm. The "red-sloping" or "RS" filter would be the opposite, with a linear slope from 0% transmission at 655 nm to 100% transmission at 685 nm. We call these 'ramp filters'. Because of this slope, the brightness through each filter is a function of the wavelength of the Hα emission line. The ratio of the light through these two filters tells us the wavelength of the Hα line, which we can use to find the redshift.

The third "continuum" filter is a 21 nm FWHM filter centered at 697 nm. This nearby filter has nearly 100% transmission, which gives us an approximation of the background light, which is then subtracted out of the other two filters. The trace for these three filters can be seen in Fig. 2.1.

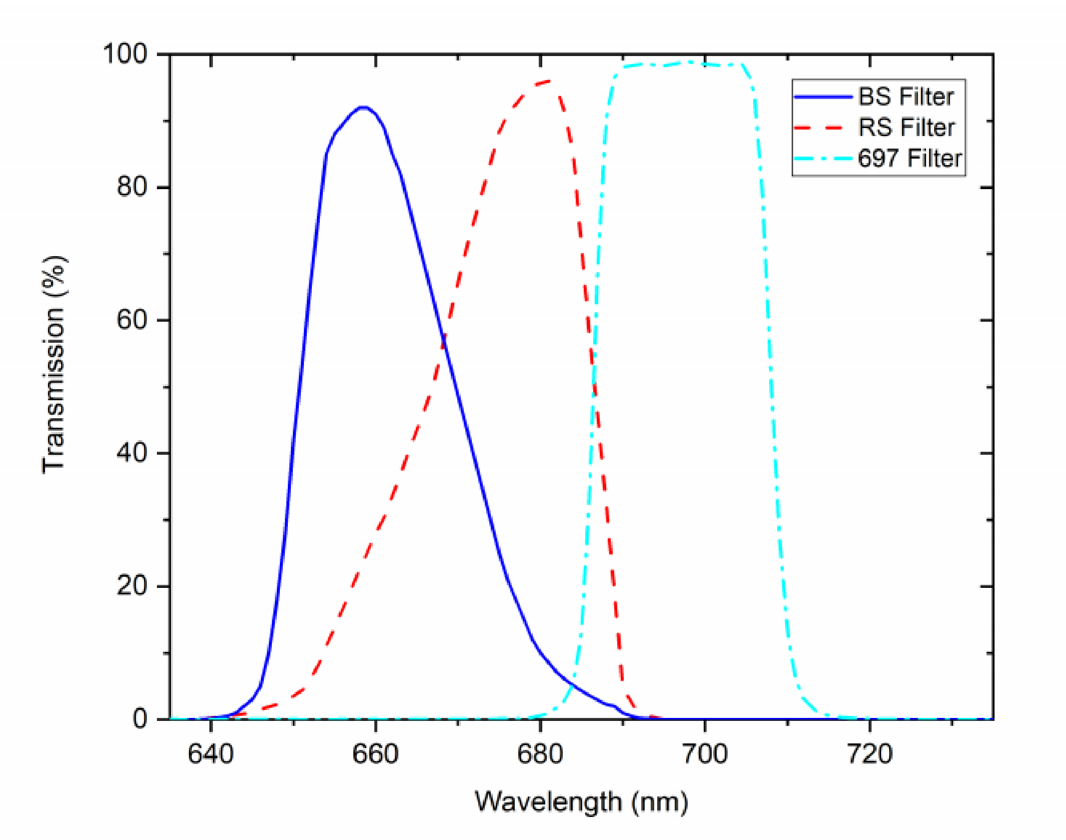

Figure 2.1 This is the filter trace for our three photometric filters. The two on the left are our "ramp" filters, where the blue-sloping (or BS) filter starts near 100% transmission for smaller wavelengths and decreases to 0% transmission for longer ones. The red-sloping (or RS) filter covers the same band of wavelengths as the BS filter, but the slope is opposite. The third "continuum" filter measures the background light, which is then subtracted from the other two filters. This figure is from Lesser et al. (2019).

2.2 Computational Modeling

We tested this method computationally using archival spectroscopic data from SDSS (see Abazajian et al. (2009)). These data came from 197 galaxies, which were each emission-line galaxies with strong Hα emission at a distance of $0.01 < z < 0.03$. For each of these galaxies, we knew the redshift (which is published by SDSS), as well as the location of the Hα line and its equivalent width. The spectrum of one of these galaxies can be found in Fig. 1.1.

2.2.1 Data Processing

We are interested in comparing the flux from the Hα line in the red-sloping (RS) filter to the flux of the Hα line in the blue-sloping (BS) filter. To find these flux values, we use the following steps:

1. We find the total flux of light through each filter, F_{total}, by integrating the flux at each wavelength $F(\lambda)$ times the filter's transmission at each wavelength $T(\lambda)$ over our wavelength range:
$$F_{total} = \int_{\lambda_{start}}^{\lambda_{end}} F(\lambda)T(\lambda)d\lambda \tag{2.1}$$
2. Next, we need an average flux value for the continuum ($F_{C_{avg}}$). We can find the average value by dividing the total flux by the width of the filter:
$$F_{C_{avg}} = \frac{F_{C_{total}}}{21nm} \tag{2.2}$$
3. We then measure the continuum's contribution to each ramp filter's flux (F_{R_C}) by inserting $F_{C_{avg}}$ in place of $F(\lambda)$ in Eq. 2.1, using $T_R(\lambda)$ as the transmission values of the ramp filter:
$$F_{R_C} = \int_{\lambda_{start}}^{\lambda_{end}} F_{C_{avg}} T_R(\lambda)d\lambda \tag{2.3}$$
4. The flux from the Hα line in each ramp filter ($F_{R_{H\alpha}}$) is the difference between each ramp filter's total flux ($F_{R_{total}}$) and continuum flux (F_{R_C}):
$$F_{R_{H\alpha}} = F_{R_{total}} - F_{R_C} \tag{2.4}$$

5. The result of step 4 is the flux from the Hα line for each of our ramp filters. By comparing the ratio of the BS filter's flux to the RS filter's flux (the BS/RS ratio) and comparing the result to the published redshifts for our galaxies, we establish the relationship between BS/RS and z. This relationship is further explored in Sec. 3.1.

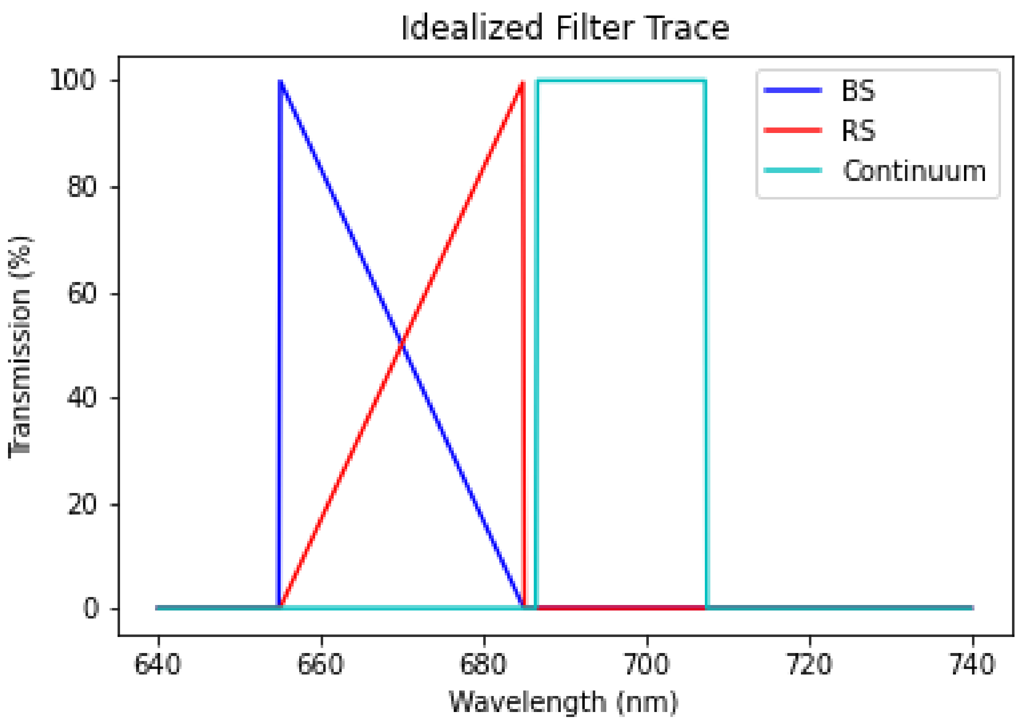

Figure 2.2 This is a filter trace for an idealized version of the filters found in Fig. 2.1. In this setup, the slopes on the BS and RS filters would be perfectly linear, and the continuum filter would have 100% transmission for its wavelength range.

2.2.2 Idealized Filter Sets

To show that our methodology was sound in the absence of imperfections, we first used an idealized version (Fig 2.2) of our actual filters (given in Fig 2.1).

While doing this method, we found a strong relationship between the BS/RS ratio and the redshift. However, for galaxies with $z > 0.018$, the [SII] emission line (doublet at $\lambda = 671.6$ nm and 673.1 nm, placing it just to the red side of Hα) is redshifted into the continuum filter. This affects our continuum measurement, and increases the error of our method. We explore the extent to which this affects our results in Chapter 3.

To adjust for this, we tried many other filter configurations, including:

- Shifting the current continuum filter so that it covers a new wavelength range of 625 nm to 645 nm.
- Two continuum filters, ranging from 625 nm to 645 nm on the blue side and from 720 nm to 740 nm on the red side. In the model, these were exposed separately to estimate the slope of the continuum.
- Two continuum filters, ranging from 625 nm to 645 nm on the blue side and from 720 nm to 740 nm on the red side. These were exposed together, giving one reading for the continuum.
- One large continuum filter, with a wavelength range of 620 nm to 720 nm.
- Narrower or wider variants of the same continuum filter (still centered on 697 nm).

Despite the change in the filters, we processed the data as outlined in 2.2.1. These configurations resulted in varying levels of success, with the best results coming from the first option. As a result, we are purchasing a new continuum filter that we hope will increase the precision of our measurements.

2.2.3 Realistic Filter Sets

After determining that our method works in ideal conditions, we repeated the computational modeling (following the steps in Sec. 2.2.1), using the transmission values of our actual (imperfect) filters (as seen in Fig 2.1). Despite the imperfections in our filters, the relationship between BS/RS and z remained strong and we believe we can accurately measure redshift using this method.

Chapter 3

Results and Conclusions

We found a strong relationship between the ratios of flux through our filters (the BS/RS ratio) and the redshift, and we found that we can predict the redshift with a standard deviation of 572 km s^{-1}, an order of magnitude more precise than similar photometric redshift methods. This relationship improves as a function of increasing Hα equivalent width, with the standard deviation dropping to 252 km s^{-1} when the equivalent width of Hα was over 40 Å. These computational results are consistent with our observations. This method requires more observational testing, and can be improved with a different continuum filter.

3.1 Results and Analysis

For each of our 197 archival galaxies, the calculated BS/RS ratio was compared to the redshift cz published by SDSS as a part of DR7 (Abazajian et al. 2009). The derived relationship is given by Eq. 3.1 below, and is graphed in Fig. 3.1.

$$cz = 6728.24\left(\frac{BS}{RS}\right)^3 - 17403.27\left(\frac{BS}{RS}\right)^2 + 8202.00\left(\frac{BS}{RS}\right) + 7201.14 \tag{3.1}$$

This relationship is valid for galaxies with cz values between 3000 and 9000 km s^{-1}, and has a standard deviation of 572 km s^{-1}. The prominent 'bump' in Fig. 3.1 at $\frac{BS}{RS} \approx 0.8$ is a known problem caused when the [SII] line is redshifted from the BS and RS filters into the continuum filter. Our proposed solution to this issue is discussed further in Sec. 3.2.

In addition to this computational modeling, we have used these filters to observe 16 active Seyfert galaxies. Our observational results closely match our computational models, indicating that our models are accurate. The results from this survey are graphed alongside the computational data in Fig. 3.1 as the "Seyfert Sample" and can also be found in Table 3.2.

Table 3.1 contains data from the 197 galaxies. The first 5 columns are published by SDSS in Abazajian et al. (2009), while the last 4 columns were calculated as part of the present investigation.

The strength of the relationship between the $\frac{BS}{RS}$ ratio and cz depended heavily upon the equivalent width of the Hα line, as shown in Fig. 3.2. We divided the galaxies into four groups: those with Hα equivalent width from 0 to 9Å, 10 to 19Å, 20 to 39Å, and greater than 40Å. The standard deviations for each of these bins, respectively, are 619, 464, 346, and 252 km s^{-1}.

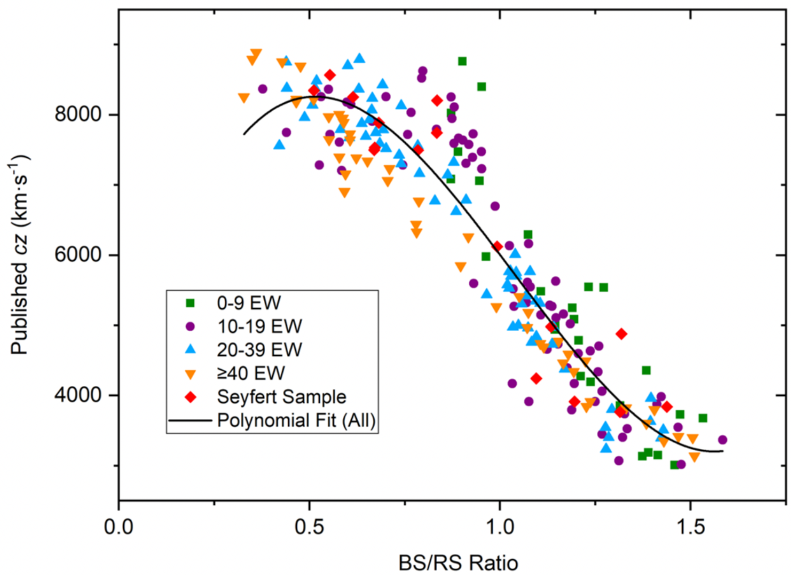

Figure 3.1 The relationship between the BS/RS ratio and the cz for galaxies with 3000 km s^{-1} < cz < 9000 km s^{-1} can be described well with a third-order polynomial fit. The data plotted here represent all 197 SDSS galaxies (separated by equivalent width of the Hα line), as well as 16 Seyfert galaxies we observed with these filters. This figure is from Lesser et al. (2019).

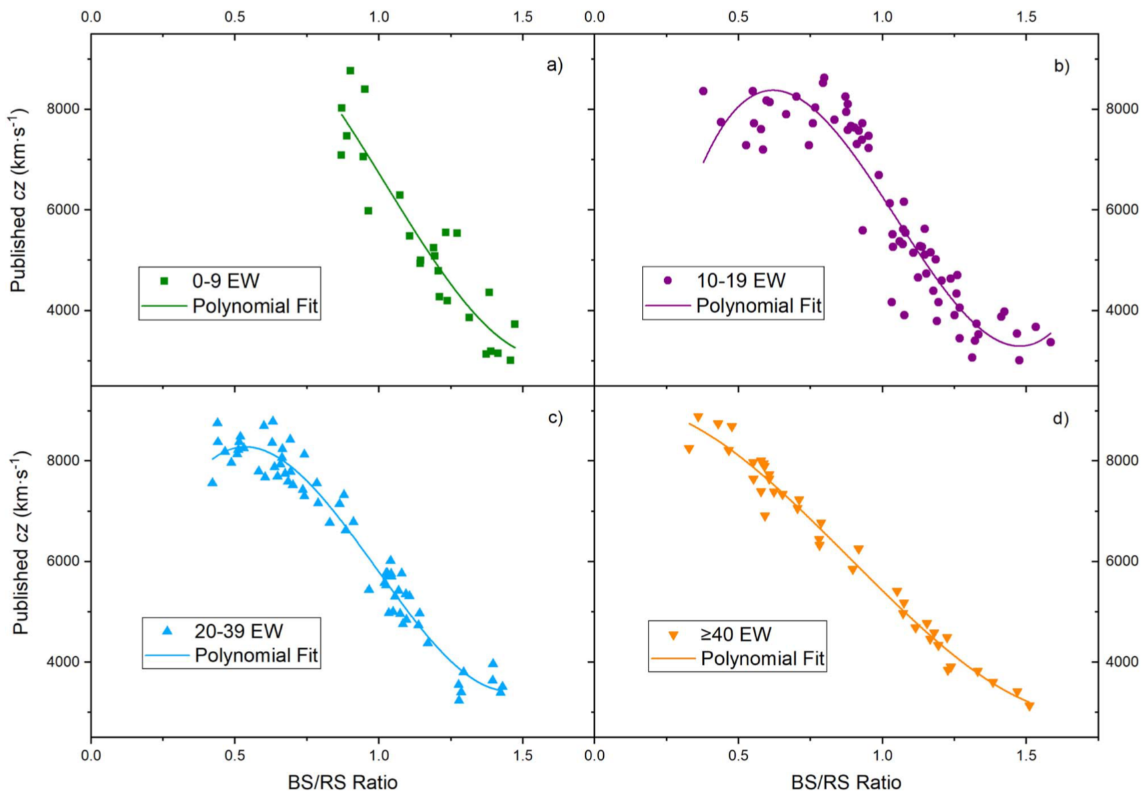

Figure 3.2 The strength of the relationship between the BS/RS ratio and *cz* increases for galaxies where the equivalent width of the Hα line is stronger. In fact, as the equivalent width increases, the relationship becomes more and more linear. This figure is from Lesser et al. (2019).

Table 3.1 Data from calculations performed on archival SDSS data for 197 galaxies. This table is from Lesser et al. (2019)

ID	RA (deg)	Decl. (deg)	z	cz (km s^{-1})	BS/RS	EW (Å)	Derived cz (km s^{-1})	Δcz (km s^{-1})
J132000.98+520303.2	200.00409130	+52.050893840	0.015290	4588	1.04400	68	4382	206
J132012.48+514554.8	200.05201480	+51.765235040	0.015780	4736	0.96800	90	4730	6
J132024.90+562613.9	200.10377330	+56.437219440	0.020440	6134	0.75600	13	6686	-552
J132035.40+340821.7	200.14752620	+34.139376230	0.023020	6909	0.39200	53	7723	-815
J132051.75+312159.8	200.21562760	+31.366615250	0.016650	4998	0.85700	25	5416	-418
J132113.04+311318.6	200.30435630	+31.221834280	0.016720	5017	0.99800	10	4853	164
J132119.66+313308.8	200.33194240	+31.552461880	0.023870	7164	0.62200	33	7014	149
J132136.07+421657.3	200.40029210	+42.282596980	0.011300	3392	1.22700	20	3325	66
J132145.44+311414.0	200.43935960	+31.237242400	0.024010	7203	0.35500	14	8523	-1320
J132202.09+311642.1	200.50873760	+31.278382460	0.024740	7425	0.49500	24	7712	-287
J132232.47+544905.5	200.63532280	+54.818203930	0.011750	3525	1.19300	15	3523	3
J132250.57+514418.0	200.71074880	+51.738336510	0.029620	8886	0.16500	62	8180	706
J132251.07+314934.3	200.71280700	+31.826220810	0.017730	5321	0.90800	15	5546	-225
J132320.14+320349.0	200.83395590	+32.063614070	0.016640	4994	0.96300	9	5123	-129
J132323.00+334326.3	200.84585230	+33.723990610	0.026680	8006	0.38700	46	7748	258
J132348.44+431804.2	200.95187420	+43.301182910	0.027270	8183	0.20800	40	8230	-47
J132353.25+512606.9	200.97191400	+51.435257350	0.025300	7591	0.62800	14	7532	59
J132412.57+414910.9	201.05240500	+41.819694910	0.024110	7233	0.48600	43	7242	-8
J132415.81+312042.4	201.06589250	+31.345120320	0.016570	4974	0.77600	26	5982	-1008
J132420.12+363545.8	201.08386630	+36.596070940	0.015890	4770	1.02200	74	4480	289
J132421.17+355449.4	201.08821950	+35.913737210	0.018420	5529	0.82000	29	5679	-151
J132440.91+310135.3	201.17047880	+31.026491210	0.023810	7143	0.61700	21	7047	96
J132513.27+535112.5	201.30530830	+53.853472400	0.025200	7560	0.61800	24	7042	519
J132523.37+593643.2	201.34740830	+59.612017160	0.026570	7972	0.35500	61	8192	-220
J132536.33+362252.4	201.40138960	+36.381234480	0.018700	5613	0.83200	18	6122	-510
J132553.81+571516.0	201.47422150	+57.254465920	0.020860	6258	0.79400	57	5601	658
J132610.81+400401.0	201.54508200	+40.066952740	0.016940	5084	1.02800	6	4712	372
J132628.53+360037.0	201.61889930	+36.010279270	0.018450	5537	1.06800	7	4379	1159
J132630.72+594313.6	201.62801790	+59.720472210	0.028960	8691	0.21300	45	8369	321
J132703.18+305836.6	201.76327360	+30.976844630	0.022570	6773	0.64700	32	6859	-86
J132719.34+314717.9	201.83062110	+31.788323500	0.015310	4594	1.05100	10	4519	75
J132742.81+532636.4	201.92840470	+53.443465620	0.029000	8701	0.36600	23	8170	531
J132747.16+510815.1	201.94651170	+51.137530650	0.025240	7574	0.74400	14	6768	806
J132804.03+333535.5	202.01680790	+33.593197990	0.024610	7385	0.48800	82	7232	152
J132833.04+320409.7	202.13766950	+32.069371950	0.015940	4783	0.95500	8	5362	-579
J132848.95+532634.4	202.20397900	+53.442910240	0.025300	7592	0.46500	38	7844	-252
J132910.96+400544.7	202.29567840	+40.095753940	0.027090	8130	0.53200	22	7532	597
J132919.40+400902.0	202.33085570	+40.150557580	0.027400	8221	0.31100	40	8118	103
J132945.90+553613.4	202.44127380	+55.603746610	0.016570	4971	0.92700	35	4941	21
J133001.76+310036.2	202.50733370	+31.010067790	0.024340	7305	0.55000	25	7436	-131
J133024.89+395949.8	202.60372510	+39.997192310	0.024090	7229	0.77000	14	6586	643
J133036.95+345502.5	202.65399770	+34.917375130	0.025570	7673	0.34100	36	8220	-547
J133040.35+325737.8	202.66813950	+32.960508900	0.024360	7308	0.70600	14	7031	277
J133044.95+321736.9	202.68733250	+32.293610410	0.022610	6785	0.71600	20	6967	-181
J133100.41+425012.5	202.75172360	+42.836807820	0.027390	8218	0.28700	80	8231	-13

ID	RA (deg)	Decl. (deg)	z	cz (km s^{-1})	BS/RS	EW (Å)	Derived cz (km s^{-1})	Δcz (km s^{-1})
J133101.60+373346.4	202.75668750	+37.562905480	0.017180	5157	0.96700	17	5090	66
J133129.97+325258.3	202.87489620	+32.882879520	0.024450	7338	0.42300	41	7568	-230
J133156.02+310158.4	202.98343570	+31.032895300	0.015520	4657	0.97900	15	4999	-342
J133227.01+365046.7	203.11254280	+36.846324160	0.022310	6695	0.79700	12	6389	305
J133248.70+415218.5	203.20291940	+41.871823220	0.027250	8177	0.37400	18	8504	-327
J133306.57+330903.7	203.27738290	+33.151051300	0.024910	7476	0.76500	14	6618	858
J133308.45+544939.1	203.28522450	+54.827534390	0.017610	5284	0.98600	12	4946	337
J133313.26+330635.1	203.30527480	+33.109762390	0.024410	7325	0.55400	27	7410	-85
J133329.90+403146.8	203.37459940	+40.529673840	0.026890	8067	0.44400	24	7929	138
J133342.58+361905.3	203.42742590	+36.318159710	0.019220	5766	0.85800	30	5413	353
J133414.81+341138.9	203.56172940	+34.194150010	0.023610	7084	0.61300	9	7538	-454
J133429.92+381738.8	203.62466690	+38.294136660	0.025730	7720	0.55300	17	7932	-212
J133451.23+340319.8	203.71348190	+34.055519210	0.025050	7518	0.42500	27	7998	-480
J133455.35+312336.5	203.73063820	+31.393489880	0.016450	4936	1.01500	7	4825	111
J133509.76+340206.3	203.79069540	+34.035083870	0.023850	7157	0.47900	232	7276	-120
J133540.80+344744.1	203.92001450	+34.795591850	0.023520	7059	0.72200	8	7193	-135
J133552.67+331937.5	203.96946200	+33.327086820	0.023540	7063	0.54200	48	6942	121
J133619.63+332524.3	204.08182760	+33.423438730	0.024900	7473	0.60700	8	7542	-69
J133659.24+333412.8	204.24685670	+33.570230010	0.025750	7728	0.43600	72	7958	-230
J133701.60+314559.4	204.25445750	+31.766509720	0.010010	3004	1.27600	8	3298	-294
J133728.90+385813.9	204.37044960	+38.970531510	0.019930	5979	0.66100	9	7446	-1466
J133817.27+481632.2	204.57199880	+48.275612710	0.027520	8257	0.08200	69	7767	490
J133851.85+475216.4	204.71604730	+47.871244710	0.027440	8234	0.47800	25	7789	445
J133935.95+430310.0	204.89979490	+43.052779320	0.011690	3509	1.25800	38	3367	142
J134009.10+365139.9	205.03795500	+36.861094510	0.019010	5703	0.82500	28	5643	61
J134018.24+320911.2	205.07602360	+32.153135670	0.025740	7725	0.73000	11	6868	857
J134100.25+422553.1	205.25104800	+42.431421940	0.027880	8366	0.37800	20	8499	-133
J134110.40+370106.9	205.29333900	+37.018597440	0.019000	5702	0.89800	23	5135	567
J134205.52+320142.8	205.52303220	+32.028576570	0.015630	4689	0.94800	66	4822	-133
J134205.95+370228.3	205.52481450	+37.041208130	0.018490	5548	1.03300	8	4670	878
J134220.18+365713.2	205.58410100	+36.953679710	0.021090	6329	0.62600	69	6494	-165
J134222.00+353726.8	205.59167810	+35.624130100	0.018060	5420	0.89400	23	5163	258
J134244.43+350346.4	205.68513950	+35.062898380	0.024280	7284	0.52600	19	8059	-775
J134313.15+364457.5	205.80479630	+36.749306710	0.019480	5847	0.75500	75	5804	43
J134447.61+313656.4	206.19837950	+31.615692660	0.027920	8378	0.18900	35	8192	186
J134448.69+370947.5	206.20289610	+37.163199750	0.026540	7963	0.26300	33	8282	-319
J134510.35+351308.6	206.29315260	+35.219080950	0.012440	3734	1.13600	10	3877	-143
J134527.23+475521.8	206.36347620	+47.922726320	0.027930	8379	0.28000	24	8512	-133
J134611.32+363548.5	206.54720050	+36.596829130	0.026480	7946	0.64400	13	7431	515
J134627.55+503838.4	206.61479720	+50.644018980	0.014580	4374	1.01500	35	4389	-15
J134650.37+423904.7	206.70988420	+42.651310740	0.028280	8484	0.34900	39	8206	279
J134701.25+335336.9	206.75524790	+33.893598260	0.016540	4962	0.87400	34	5305	-342
J134706.93+335249.9	206.77890190	+33.880540460	0.014860	4459	1.00700	63	4548	-89
J134714.45+553410.0	206.81022510	+55.569471140	0.015430	4631	1.08900	12	4193	438
J134750.05+374500.9	206.95855450	+37.750252970	0.018390	5518	0.77100	16	6575	-1057
J134835.96+333042.6	207.14987330	+33.511860240	0.014450	4336	0.98200	13	4979	-642
J134840.49+312739.1	207.16872830	+31.460887020	0.026300	7891	0.45100	62	7421	470
J134908.64+532207.5	207.28602970	+53.368755950	0.029170	8753	0.22900	35	8261	493
J134935.08+351511.6	207.39616790	+35.253247400	0.017150	5147	0.94500	10	5262	-115

ID	RA (deg)	Decl. (deg)	z	cz (km s^{-1})	BS/RS	EW (Å)	Derived cz (km s^{-1})	Δcz (km s^{-1})
J134939.77+474907.9	207.41574800	+47.818887770	0.027870	8362	0.26800	15	8496	-134
J135026.98+321706.6	207.61243810	+32.285180740	0.025460	7638	0.67800	11	7216	422
J135032.73+350753.8	207.63639230	+35.131628140	0.020970	6293	0.87400	6	6093	200
J135054.20+381629.2	207.72587300	+38.274796000	0.011340	3402	1.14400	30	3726	-334
J135147.20+505841.9	207.94670780	+50.978330110	0.013260	3979	1.22400	11	3346	633
J135221.23+381145.2	208.08849380	+38.195893810	0.018750	5627	0.89500	12	5643	-16
J135231.95+374902.6	208.13315150	+37.817415570	0.012100	3631	1.22800	32	3436	195
J135307.77+341811.1	208.28241300	+34.303104850	0.026490	7950	0.39600	41	8090	-140
J135314.23+381337.7	208.30931920	+38.227148830	0.011380	3414	1.25400	40	3555	-141
J135338.89+573331.8	208.41204420	+57.558851500	0.025970	7794	0.64300	12	7439	354
J135341.69+573120.1	208.42373370	+57.522259260	0.025970	7792	0.37700	39	8142	-350
J135402.47+543706.6	208.51029520	+54.618518220	0.025550	7666	0.71300	14	6987	679
J135604.45+381815.0	209.01854480	+38.304181580	0.018650	5596	0.69100	17	7339	-1744
J135637.76+361445.9	209.15737130	+36.246090380	0.017010	5105	0.94700	10	5242	-136
J135714.98+343037.5	209.31245170	+34.510437090	0.027020	8109	0.64500	12	7425	684
J135834.11+372709.9	209.64215880	+37.452768370	0.011330	3401	1.23200	12	3299	102
J135930.58+384734.7	209.87743240	+38.792994500	0.018270	5483	0.92900	6	5599	-116
J135943.14+402312.0	209.92977080	+40.386677470	0.012660	3799	1.28400	248	3503	296
J135947.77+402255.9	209.94904720	+40.382214790	0.012630	3791	0.98900	16	4927	-1136
J140021.16+385504.2	210.08818760	+38.917843680	0.017560	5268	1.03600	17	4571	697
J140043.62+315338.0	210.18175530	+31.893912480	0.014630	4391	1.01400	14	4737	-347
J140045.79+300433.5	210.19081980	+30.075974700	0.027150	8146	0.35100	17	8527	-381
J140056.38+410026.8	210.23493140	+41.007453980	0.012670	3801	1.15200	28	3693	109
J140106.73+343451.2	210.27804410	+34.580915660	0.027510	8253	0.62000	10	7531	722
J140141.38+334936.5	210.42244590	+33.826822210	0.026350	7906	0.41300	19	8435	-529
J140236.34+345120.4	210.65144860	+34.855682650	0.013200	3961	1.16600	29	3636	325
J140310.03+384606.0	210.79180590	+38.768339400	0.019180	5756	0.82300	21	5654	103
J140420.13+505504.1	211.08391570	+50.917812790	0.026430	7931	0.47500	26	7801	130
J140436.98+353243.8	211.15408880	+35.545505600	0.013970	4193	1.06000	8	4443	-251
J140447.98+304437.3	211.19995740	+30.743699550	0.025190	7558	0.14500	35	8063	-505
J140450.12+310354.4	211.20887110	+31.065131650	0.014450	4337	1.03100	49	4439	-102
J140640.83+351647.7	211.67013910	+35.279935960	0.013880	4167	1.03300	19	4599	-433
J140759.59+313845.9	211.99830620	+31.646089390	0.016550	4968	0.88500	72	5133	-165
J140902.00+361924.2	212.25833560	+36.323412980	0.010770	3232	1.06900	25	4084	-852
J140907.45+464710.0	212.28104990	+46.786114500	0.013020	3909	1.07100	50	4267	-358
J140947.13+553558.3	212.44640410	+55.599544880	0.025950	7786	0.50700	33	7656	131
J141002.10+373303.4	212.50878360	+37.550968990	0.026260	7878	0.45500	36	7886	-8
J141035.90+592128.7	212.64960160	+59.357994000	0.010220	3067	1.13400	15	3889	-823
J141055.49+394619.7	212.73123950	+39.772149210	0.018600	5580	0.75600	33	6684	-1103
J141226.51+454125.4	213.11049020	+45.690408710	0.027130	8139	0.30800	33	8264	-125
J141235.85+461218.8	213.14938320	+46.205227850	0.015770	4731	0.99300	15	4890	-201
J141333.52+395305.7	213.38969610	+39.884932190	0.018480	5546	0.82200	16	6196	-651
J141349.19+371608.8	213.45497730	+37.269113280	0.022070	6624	0.63300	30	6946	-322
J141353.52+455213.7	213.47302790	+45.870492250	0.027520	8256	0.53000	19	8039	217
J141414.77+352525.1	213.56154540	+35.423661990	0.010490	3147	1.13200	9	3902	-755
J141508.07+453541.4	213.78366370	+45.594850150	0.015850	4757	0.92800	22	4937	-179
J141538.37+362230.2	213.90987590	+36.375074920	0.015670	4703	1.07700	10	4278	425
J141544.84+361041.6	213.93685850	+36.178224030	0.024640	7392	0.75000	10	6727	666
J141545.72+400619.2	213.94051780	+40.105335870	0.020030	6011	0.83500	22	5570	441

ID	RA (deg)	Decl. (deg)	z	cz (km s^{-1})	BS/RS	EW (Å)	Derived cz (km s^{-1})	Δcz (km s^{-1})
J141605.64+320751.3	214.02352800	+32.130942250	0.028000	8401	0.72300	7	7190	1211
J141623.86+393007.8	214.09942970	+39.502190230	0.019240	5774	0.80800	23	5758	16
J141631.09+574836.6	214.12954660	+57.810173730	0.010440	3132	1.20000	8	3523	-457
J141722.07+573747.5	214.34198760	+57.629866070	0.010040	3013	1.26600	16	3125	-112
J141816.38+365300.8	214.56826560	+36.883576360	0.011210	3366	1.33300	10	3308	57
J141921.31+350531.7	214.83882200	+35.092161890	0.028080	8426	0.46700	21	7835	591
J141934.02+402010.3	214.89176100	+40.336211540	0.025470	7642	0.43600	48	7498	144
J141935.29+360826.4	214.89707460	+36.140668370	0.024650	7397	0.37400	83	7815	-418
J141936.98+381403.3	214.90409790	+38.234257840	0.020540	6163	0.89700	14	5628	536
J141943.23+491411.9	214.93012830	+49.236645600	0.025490	7647	0.28800	51	8278	-631
J141954.49+515340.3	214.97706180	+51.894555110	0.029170	8752	0.25000	71	8400	352
J142001.84+353916.1	215.00767070	+35.654476790	0.011810	3544	1.11000	30	3875	-330
J142026.48+351119.6	215.11034900	+35.188799040	0.011800	3542	1.27200	15	3098	445
J142055.01+400715.6	215.22922900	+40.121025460	0.017480	5246	0.96600	7	5267	-21
J142121.49+362540.5	215.33956860	+36.427934730	0.011150	3347	1.31200	292	3427	-80
J142152.59+395844.7	215.46914730	+39.979094220	0.017260	5180	0.85500	49	5282	-102
J142237.07+595551.1	215.65447040	+59.930878190	0.029200	8761	0.65000	5	7477	1284
J142308.04+501316.9	215.78350870	+50.221377640	0.026780	8034	0.52600	16	8057	-23
J142342.38+340032.4	215.92659550	+34.009018780	0.012730	3821	1.16500	56	3895	-74
J142406.49+345154.0	216.02708190	+34.865014700	0.012910	3875	1.13600	17	3873	2
J142430.49+570815.6	216.12706080	+57.137686920	0.010440	3135	1.37200	58	3286	-151
J142451.30+381511.9	216.21378370	+38.253307590	0.021460	6439	0.56600	74	6819	-380
J142603.47+384632.8	216.51446740	+38.775800030	0.016130	4842	0.93300	35	4904	-63
J142658.50+313101.3	216.74378610	+31.517046400	0.012850	3856	1.11000	6	4053	-198
J142709.50+305653.5	216.78959730	+30.948207550	0.013520	4057	1.10900	12	4057	1
J142713.49+503344.6	216.80623450	+50.562411040	0.013030	3910	1.07600	17	4286	-376
J142737.14+402426.3	216.90478100	+40.407321410	0.019210	5765	0.90100	20	5119	646
J142829.67+362909.4	217.12363530	+36.485959730	0.029300	8791	0.13100	90	8002	788
J142900.21+355637.5	217.25091090	+35.943768280	0.014970	4491	1.04600	42	4373	18
J142907.85+325436.6	217.28274380	+32.910184830	0.014240	4272	1.03700	8	4631	-359
J142908.34+414950.8	217.28477160	+41.830790080	0.017910	5373	0.79100	14	6434	-1060
J142909.77+314755.3	217.29073950	+31.798703780	0.011480	3446	1.07700	15	4277	-830
J142911.68+300438.0	217.29869850	+30.077236540	0.014510	4355	1.18400	7	3596	759
J142934.48+493815.1	217.39367720	+49.637543070	0.012800	3842	1.14200	58	3982	-140
J142949.76+343605.5	217.45736500	+34.601551030	0.028740	8624	0.62300	12	7557	1068
J143009.65+311257.0	217.54023940	+31.215835220	0.011320	3398	1.40500	250	3222	177
J143052.33+551440.0	217.71805770	+55.244465720	0.017540	5263	0.85800	86	5266	-4
J143117.95+472951.4	217.82483240	+47.497611370	0.026740	8022	0.64200	8	7496	526
J143125.36+331349.8	217.85567300	+33.230517200	0.022560	6769	0.63800	77	6427	342
J143125.86+304713.1	217.85775180	+30.786993760	0.011990	3599	1.20600	83	3749	-150
J143200.92+361818.7	218.00384220	+36.305204340	0.012410	3726	1.16300	9	3710	16
J143312.67+411913.8	218.30283090	+41.320500360	0.018120	5436	0.77900	32	5968	-531
J143333.58+404816.6	218.38995390	+40.804638080	0.017670	5303	0.89000	24	5193	111
J143346.83+400451.2	218.44513600	+40.080912350	0.025350	7607	0.26900	16	8498	-891
J143348.35+400538.9	218.45147280	+40.094156200	0.025820	7748	0.43900	23	8371	-623
J143518.38+350707.4	218.82659170	+35.118738210	0.028410	8523	0.59900	14	7696	827
J143632.05+414109.1	219.13358320	+41.685876950	0.018020	5409	0.82600	60	5430	-21
J143638.71+410444.8	219.16132470	+41.079126600	0.015760	4730	0.98500	38	4648	82
J143639.94+410937.3	219.16642730	+41.160369750	0.017700	5312	0.85400	28	5440	-128

ID	RA (deg)	Decl. (deg)	z	cz (km s^{-1})	BS/RS	EW (Å)	Derived cz (km s^{-1})	Δcz (km s^{-1})
J143713.57+434145.3	219.30656550	+43.695943630	0.010620	3187	1.13200	7	3904	-717
J143756.49+481233.9	219.48540760	+48.209443900	0.025640	7692	0.43800	27	7950	-258
J143758.75+412033.0	219.49482910	+41.342517250	0.017820	5347	0.93100	24	4915	432
J143838.26+541640.2	219.65944230	+54.277841020	0.029300	8792	0.43600	24	7960	831
J143850.01+302633.1	219.70840520	+30.442527940	0.012240	3674	1.29300	9	3284	391

Table 3.2 Data from the 16 galaxies surveyed using ramp filters. This table is adapted from Lesser et al. (2019)

Galaxy	Type	B_{mag} (mag)	cz (km s^{-1})	BS/RS	Derived cz (km s^{-1})	Δcz (km s^{-1})
Mrk 686	Sey 2	14.55	4242	0.901	4121	-121
NGC 5548	Sey 1	14.35	4877	1.124	4739	-138
Mrk 266SW	LINER	14.19	8564	0.359	8297	-267
NGC 6786	Sey 2	13.70	7500	0.475	7949	449
NGC 2650	Sey 2	14.30	3839	1.243	4054	215
NGC 5765	Sey 2	14.60	8345	0.317	7968	-376
NGC 5990	Sey 2	13.10	3765	1.120	4047	282
NGC 6521	Sey 2	14.30	8202	0.640	7251	-951
Z 229-015	Sey 1	15.40	8253	0.420	8212	-41
Z 493-002	Sey 2	15.60	7529	0.477	8100	572
Mrk 461	Sey 2	14.50	4977	0.940	4415	-562
NGC 5674	Sey 2	13.70	7493	0.590	7395	-98
IC 1368	Sey 2	14.30	3912	1.001	4666	754
II ZW 102	Sey 2	15.39	7885	0.487	7680	-205
NGC 3822	Sey 2	13.70	6122	0.798	5788	-333
NGC 5515	Sey 2	13.70	7743	0.639	6931	-812

3.2 Future Work

Our current continuum filter is a 21 nm FWHM filter centered at 697 nm. This works decently well to remove the continuum from our BS and RS filters, but for galaxies with $z > 0.018$ the [SII] line is redshifted into the continuum filter and greatly increases our errors. After computationally modeling many different filter layouts to find a suitable replacement (see Sec. 2.2.2), we found that the best continuum filter would be identical to our current figure, but shifted blueward of our BS and RS filters. We are going to obtain this filter to use in future survey work.

Our preliminary observational results support the accuracy of our models, but more observations with these filters are needed to confirm the method. Future observations with these filters should compare calculated cz values with those obtained spectroscopically to verify their validity.

As described in Chapter 1, these filters are useful for survey work, particularly for dwarf galaxies within voids. We plan to one day use these filters to conduct a survey of nearby voids in an effort to identify the first known void galaxy.

Bibliography

Abazajian, K. N., Adelman-McCarthy, J. K., Agueros, M. A., Allam, S. S., & Prieto, C. A. 2009, The Astrophysical Journal Supplement, 182, 543

Baum, W. A. 1962, in Problems of Extra-Galactic Research, ed. G. C. McVittie, Vol. 15, 390

Beck, R., Dobos, L., Budavári, T., Szalay, A. S., & Csabai, I. 2016, MNRAS, 460, 1371

Bolzonella, M., Miralles, J. M., & Pelló, R. 2000, A&A, 363, 476

Carrasco Kind, M., & Brunner, R. J. 2013, MNRAS, 432, 1483

Collister, A. A., & Lahav, O. 2004, PASP, 116, 345

Connolly, A. J., Csabai, I., Szalay, A. S., Koo, D. C., Kron, R. G., & Munn, J. A. 1995, AJ, 110, 2655

Koo, D. C. 1985, AJ, 90, 418

Leavitt, H. S. 1908, Annals of Harvard College Observatory, 60, 87

Lesser, R. W., Moody, J. W., Steele, J., Bohman, J., McNeff, M., Joner, M. D., & Barnes, J. 2019, AJ, 157, 99

Loh, E. D., & Spillar, E. J. 1986, ApJ, 303, 154

Pello, R., Miralles, J. M., Le Borgne, J. F., Picat, J. P., Soucail, G., & Bruzual, G. 1996, A&A, 314, 73

Tully, R. B., de Marseille, O., & Fisher, J. R. 1975, in Bulletin of the American Astronomical Society, Vol. 7, 426

Index